Computational Materials Science 137 (2017) 6–9

Contents lists available at ScienceDirect

Computational Materials Science

journal homepage: www.elsevier.com/locate/commatsci

First principles study of Cr poisoning in solid oxide fuel cell cathodes: Application to (La,Sr) CoO_3

Sridevi Krishnan [a,b,d,*], Manoj K. Mahapatra [c], Prabhakar Singh [a,d], Rampi Ramprasad [a,b]

[a] Materials Science and Engineering, University of Connecticut, Storrs, CT, USA
[b] Institute of Materials Science, University of Connecticut, Storrs, CT, USA
[c] Department of Materials Science and Engineering, University of Alabama at Birmingham, AL, USA
[d] Center for Clean Energy Engineering, University of Connecticut, Storrs, CT, USA

ARTICLE INFO

Article history:
Received 28 November 2016
Received in revised form 18 April 2017
Accepted 20 April 2017

Keywords:
Density functional theory
First principles thermodynamics
Solid oxide fuel cells
Cr poisoning

ABSTRACT

Solid oxide fuel cell (SOFC) systems provide efficient and clean power. Chromium poisoning is known to deteriorate the performance of the SOFC cathodes such as $La_{1-x}Sr_xCoO_3$ (LSCO) due to the formation of undesired products. We identify the reaction products when LSCO is in a CrO_3 and O_2 atmosphere using first principle thermodynamics, with the assumption that gas-phase CrO_3 is the Cr source. Our results correctly identify $SrCrO_4$ as the primary Cr poisoning product as observed in experiments and also provides temperature-pressure regimes under which Cr poisoning effects may be avoided.

Solid oxide fuel cells (SOFC) are complex electrochemical systems offering an efficient and clean route for energy conversion. Typically, doped perovskite oxides such as $La_{1-x}Sr_xMnO_3$ (LSMO) [1–3] and $La_{1-x}Sr_xCoO_3$ (LSCO) derivatives [4–9] are widely used as cathode materials in SOFCs [10]. Generally, these cathodes undergo performance deterioration due to a Cr deposition process known as Cr poisoning [11–15]. The most dominant Cr deposition product is observed to be $SrCrO_4$ [16–19] for LSCO based cathodes. It is necessary to understand the conditions and compositions at which these compounds form. Here we present a systematic study of the reaction energetics between the LSCO cathodes and the representative Cr species at SOFC operating conditions and provide valuable insights into the Cr poisoning process.

The volatile Cr species in the SOFC atmosphere is at the core of the detrimental effects of Cr poisoning. It has been observed that the volatile Cr species strongly depends on the oxygen partial pressure and the water content in the environment. CrO_3, the most dominant vapor species over the Cr_2O_3 scale [17] in dry air, is chosen as the representative Cr species in this study.

First principles calculations offer a powerful route for the systematic study of such complex phenomena [20–25]. We study the bulk reaction thermodynamics between a set of reactants (i.e., LSCO and CrO_3) to find the thermodynamically favorable reaction pathway as a function of temperature (T) and CrO_3 partial pressure (P_{CrO_3}). We correctly identify the experimentally known dominant Cr deposition products, $SrCrO_4$ and Co_3O_4, thus validating our approach. Additionally, this method accomplishes the following: (1) It identifies the P-T conditions to avoid Cr-poisoning and (2) it offers a strategy for determining the reaction energetics in other related situations, e.g., Cr poisoning of LSMO, BSCF ($Br_{0.5}Sr_{0.5}Co_{0.8}Fe_{0.2}O_3$) [26] cathodes.

The crystal structure of $La_{1-x}Sr_xCoO_3$ undergoes a rhombohedral ($x \leqslant 0.55$) to cubic ($x > 0.55$) transition with increasing Sr concentration [27]. Typically, higher concentration of Sr [28] ($x = 0.4$) is used in LSCO based cathodes. Therefore, in this study we chose the compound $La_{0.5}Sr_{0.5}CoO_3$ ($x = 0.5$), which is cubic at the high operating temperature encountered in SOFCs [29,30]. A thermodynamically favorable reaction pathway is obtained by combining a linear programming method with first principles thermodynamics. Our approach assesses all possible products of a set of reactants and arrives at the energetically favorable set of products. The reaction free energy is then obtained from the newly identified set of products which is then translated into the phase diagram at experimental P-T conditions.

For our particular reaction of interest (see Table 1), the element space defined by our reactants consists of La, Sr, Co, Cr and O. A product pool is then created comprising of all possible reaction products such as the elemental metal, binary oxides, ternary oxides

* Corresponding author at: Institute of Materials Science, University of Connecticut, Storrs, CT, USA.
E-mail address: sridevikrish@gmail.com (S. Krishnan).

http://dx.doi.org/10.1016/j.commatsci.2017.04.020
0927-0256/

Table 1
The thermodynamically favorable decomposition pathway.

Reactants	Product pool
$La_{1-x}Sr_xCoO_3$, CrO_3	La, Sr, Co, Cr, La_2O_3, SrO, Co_3O_4, Cr_2O_3, $LaCoO_3$, $La_{0.5}Sr_{0.5}CoO_3$, $LaCrO_3$, $CoCr_2O_4$, $SrCrO_4$, O_2

Reaction

$$\begin{aligned} La_{1-x}Sr_xCoO_3 + \alpha CrO_3 \rightarrow\ & c_1La + c_2Sr + c_3Co + c_4Cr + c_5La_2O_3 + c_6SrO \\ & + c_7Co_3O_4 + c_8Cr_2O_3 + c_9LaCoO_3 \\ & + c_{10}La_{0.875}Sr_{0.125}CoO_3 + c_{11}LaCrO_3 \\ & + c_{12}CoCr_2O_4 + c_{13}SrCrO_4 + c_{14}O_2 \end{aligned} \quad (1)$$

α is the concentration of CrO_3 in the reaction and the c_is (i = 1–14) are the balancing coefficients for each of the products respectively.

Quantity to minimize (c_i)

$$E_P = \min_{c_i}\left\{\sum_{i=1}^{n} c_i E_i + c_{(i=n+1)}\mu_{O_2}\right. \quad (2)$$

c_i, n and E_i represents balancing coefficient, the number of products in the pool excluding O_2 & their corresponding DFT energies respectively. $\mu_{O_2} = E_{O_2} + \Delta\mu_{O_2}$ where, E_{O_2} is the DFT energy of an isolated O_2 molecule.

$$\Delta\mu_{O_2}(T,p) = \Delta\mu_{O_2}(T,p^0) + k_B T \ln\left(\frac{p_{O_2}}{p^0}\right) \quad (3)$$

Here T, p, p^0, p_{O_2} and k_B are the temperature, pressure, standard pressure (= 1 atm), O_2 partial pressure and Boltzmann constant respectively.

Constraints

$$\sum_{i=1}^{n+1} c_i s_i^e = s^e; \quad \forall 1 \leqslant e \leqslant n_{elem} \quad (4)$$

s_i^e, s^e is the proportion of element 'e' in the product 'i' & in the reactants respectively. n_{elem} is the number of elements in the element space.

Free energy of reaction (F_R)

$$F_R = E_P - E_{La_{1-x}Sr_xCoO_3} - \alpha(E_{CrO_3} + \Delta\mu_{CrO_3}) \quad (5)$$

$E_P, E_{La_{1-x}Sr_xCoO_3}$ and E_{CrO_3} are the minimized energy of products, energies of $La_{1-x}Sr_xCoO_3$ and isolated CrO_3 molecule respectively. α and $\Delta\mu_{CrO_3}$ are the concentration and chemical potential of CrO_3 respectively.

$$\Delta\mu_{CrO_3}(T,p) = \Delta\mu_{CrO_3}(T,p^0) + k_B T \ln\left(\frac{p_{CrO_3}}{p^0}\right) \quad (6)$$

Here T, p, p^0, p_{CrO_3} and k_B are the temperature, pressure, standard pressure (= 1 atm), CrO_3 partial pressure and Boltzmann constant respectively.

and oxygen including the chromates (Table 1). Thus, we now have a reaction (Eq. (1)) with a variable α (concentration of CrO_3) on the reactant side and coefficients (c_i) preceding each of the products whose values are unknown. The thermodynamically favorable set of products can be obtained once the value for each of these coefficients has been solved as function of α values.

The linear programming (LP) method offers an efficient approach to find the most energetically favorable decomposition pathway for the reactions without explicitly identifying all possible reaction pathways and comparing them. The optimized energy of the products (E_P) of the reaction between $La_{0.5}Sr_{0.5}CoO_3$ + αCrO_3 is obtained by minimizing Eq. (2) subject to the stoichiometry preservation constraints in Eq. (4) in Table 1. Here again, the product energy E_P depends on the oxygen chemical potential and assuming ideal gas behavior, it can be related to its partial pressure according to Eq. (3). The oxygen chemical potential ($\Delta\mu_{O_2}$) can be determined using statistical thermodynamics [25,31] or the JANAF data [32]. The oxygen partial pressure is fixed at 0.2 atm in accordance with the experimental SOFC conditions for all our calculations. Thus, in the calculation of free energy, the entropic contributions are included only for the gaseous species CrO_3 and O_2. The summation in Eq. (4) is done for each element in the element space (i.e., La, D, Mn, Cr and O). For example, in case of the element La, the variables s^e and s_i^e in Eq. (4) becomes s^{La} and s_i^{La} for the ith product in the pool. Then, $s^{La} = 0.5$ and $s_5^{La} = 2$, the proportion of La in the reactant $La_{0.5}Sr_{0.5}CoO_3$ and the 5th product La_2O_3 in the pool respectively (refer Table 1).

Then the free energy of the reaction (Eq. (1)) can be obtained as defined in Eq. (5) as a function of CrO_3 chemical potential. Assuming ideal gas behavior, the CrO_3 chemical potential can be related to its partial pressure according to Eq. (6). The CrO_3 chemical potential ($\Delta\mu_{CrO_3}$) can be determined using statistical thermodynamics [25,31] or the JANAF data [32]. The change in the concentration of CrO_3 alters the reaction pathway which in turn affects the free energy of the reaction. We systematically study the reaction energetics between CrO_3 and $La_{0.5}Sr_{0.5}CoO_3$ for a large number of CrO_3 concentrations (α) ranging from 0 to 1 and the temperature from 800 to 1500 K from which the phase diagram is constructed. Although the reaction kinetics also plays a vital role, it is important to recognize that our approach provides decomposition pathways based solely on the reaction energetics.

All energies of the reactants and products are obtained from spin polarized calculations using DFT as implemented in the VASP [33,34] code. The exchange correlation is treated using the generalized gradient approximation (GGA) with Perdew-Burke-Ernzerhof (PBE) [35] functional. The projector augmented wave (PAW) potentials [36] were used to describe the core states. All calculations were performed with a cutoff energy of 520 eV and a Monkhorst-Pack k-point grid with a spacing of at least 0.13 $Å^{-1}$ was used to sample the Brillouin zone. The atomic positions were relaxed until the force on each atom fell below a threshold of 0.02 eV/Å. $La_{0.5}Sr_{0.5}CoO_3$ was relaxed in the cubic structure while the ground state structures were considered for the rest of the compounds. A shift of 1.38 eV/O_2 molecule is used to destabilize the total energy of the O_2 molecule (E_{O_2} (corrected) = −8.48 eV) to account for the overbinding of the oxygen molecule in the GGA-PBE level of theory, consistent with previous results [37–39]. It is well known that the treatment based on the semilocal GGA functionals are insufficient for the of highly correlated oxides considered here [40]. DFT + U is generally employed to overcome this issue however identifying an optimal value of U for the transition metals in different chemical environment is questionable [41]. Moreover, hybrid functionals are computationally expensive therefore we employ a consistent GGA-PBE level of theory across all products.

To understand the energetics of the different set of products with the CrO_3 concentration, the free energy of the reaction (F_R in Eq. (5)) between CrO_3 and $La_{0.5}Sr_{0.5}CoO_3$ at 900 K is shown in Fig. 1(a). The color gradient represents the slope (value of α) of the lines. Colors from blue to red corresponds to α values from 0 to 1, respectively. The lowest free energy at various $\Delta\mu_{CrO_3}$ and their corresponding α values are obtained for the temperature range of interest.

The c_i values corresponding to the CrO_3 concentration (α) of interest at 900 K is shown in Fig. 1(b). The columns without any bubble correspond to c_i values of zero and the ones with the bubble correspond to the thermodynamically favorable product with the bubble sizes representing the amount of that product. It is imme-

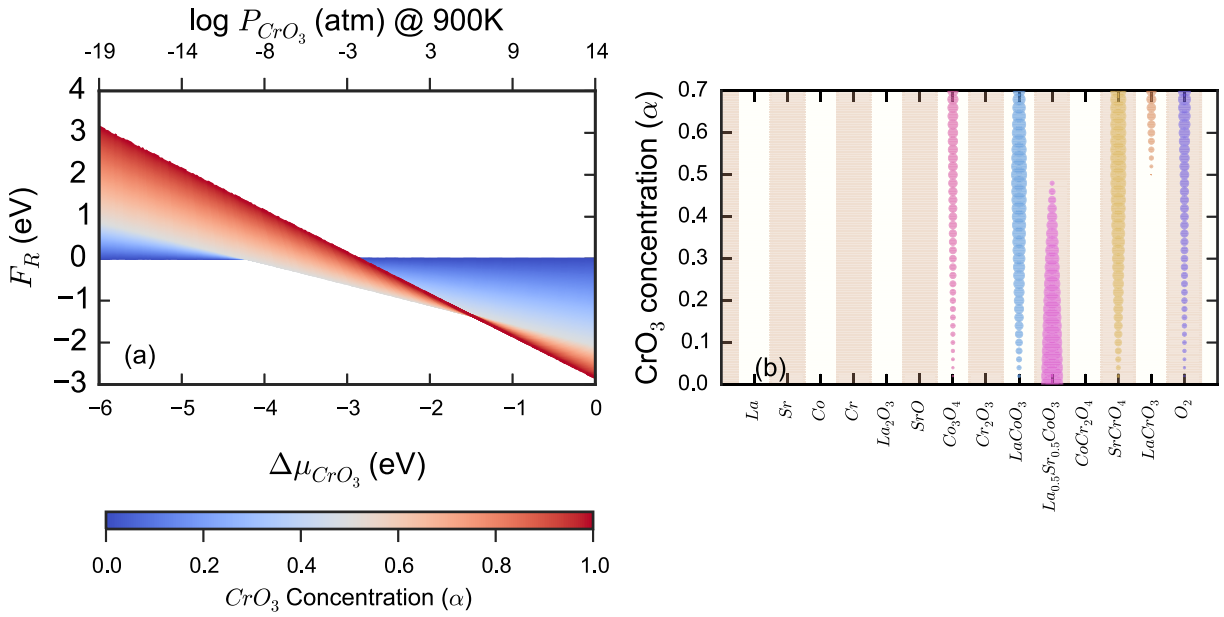

Fig. 1. Thermodynamics of the reaction between $La_{0.5}Sr_{0.5}CoO_3$ and CrO_3 (a) The free energy of the reaction (F_R) at 900 K as function of $\Delta\mu_{CrO_3}$. The colored lines represent the F_R for each value of α. The blue to red lines represent α values from 0 to 1 respectively. (b) Bubble chart representing the c_i for products in the product pool for increasing concentration of CrO_3 (α). The size of the bubbles represent the amount of that particular product and the y axis shows the changing α values. (For interpretation of the references to color in this figure legend, the reader is referred to the web version of this article.)

diately evident that the reaction pathway is altered with increasing CrO_3 concentration (α) values along with the change in the amounts of the products. It is clear that the $La_{0.5}Sr_{0.5}CoO_3$ is stable and remains undisturbed in the absence of Cr vapor ($\alpha = 0$). The Cr reaction products begin to appear with increasing concentrations of CrO_3. Interestingly, we find that the by-product of Cr poisoning, $SrCrO_4$, appears in the thermodynamic reaction pathway and the amount of the compound in the product increases with increasing α values. Although, the other Cr-Co compound $CoCr_2O_4$ is present in the product pool, it does not appear as a thermodynamically favorable product.

Based on the chemical potentials and the corresponding thermodynamically favorable products, the phase diagram of reaction for a range of experimentally observable temperature and CrO_3 partial pressures (P_{CrO_3}) (Fig. 2) is constructed. We have identified

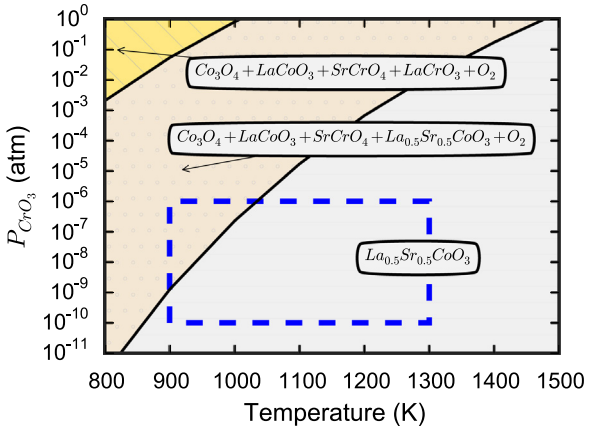

Fig. 2. Phase diagram for the reaction between $La_{0.5}Sr_{0.5}CoO_3$ and CrO_3. The thermodynamically favorable products in different $P_{CrO_3} - T$ range are indicated in the plot. The blue rectangle represents the window of experimental temperature and CrO_3 partial pressure. (For interpretation of the references to color in this figure legend, the reader is referred to the web version of this article.)

the window of experimental P_{CrO_3}-T conditions based on the measurement of chromium evaporation rate in the SOFC atmosphere of different chromia forming alloys (the source of chromium) [17,42]. In this window of experimentally observed temperature and pressure (blue dotted rectangle in Fig. 2), the energetics of the interaction between $La_{0.5}Sr_{0.5}CoO_3$ and CrO_3 can be classified as the reactive and the non-reactive sections. In the reactive sections, the pathway for the reaction between CrO_3 and $La_{0.5}Sr_{0.5}CoO_3$ proceeds to form products such as Co_3O_4, $SrCrO_4$, $LaCoO_3$ and O_2 coexisting with the reactant, $La_{0.5}Sr_{0.5}CoO_3$ at experimental P_{CrO_3}-T conditions. However, at low P_{CrO_3} and high temperatures the LSCO compound remains unreacted (Fig. 2).

We find that for the stoichiometric LSCO, the thermodynamically favorable pathway includes the formation of the experimentally observed Cr poisoning products, $SrCrO_4$ and Co_3O_4. Our results show that the formation of $SrCrO_4$ is energetically favorable over the formation of $CoCr_2O_4$. This is in line with experimental observations where only $SrCrO_4$ [16] is observed as the Cr poisoning product, further validating our finding.

The formation of the Cr poisoning product $SrCrO_4$ in the reaction phase diagram (Fig. 2) determines the P-T conditions to avoid Cr poisoning effects. The Cr poisoning effects are dominant at the cathode surfaces, however, we focus on the bulk thermodynamics to determine the optimal Cr concentration which makes the Cr poisoning process possible. Thereby providing guidelines of the threshold Cr partial pressure to avoid the detrimental effects. Accordingly, at ≈900 K, the $La_{0.5}Sr_{0.5}CoO_3$ remains unreacted at low CrO_3 partial pressures ($< 10^{-9}$ atm), however, with increasing CrO_3 partial pressure, it readily reacts. On the other hand, with increasing temperature higher concentrations of CrO_3 are accommodated without reaction. For instance, at temperatures above ≈1050 K, LSCO remains unreacted even for a higher CrO_3 partial pressure of $\approx 10^{-6}$ atm. Therefore, our findings provide good guidelines for the experimental P-T range to avoid effects of Cr poisoning in LSCO.

The bulk reaction thermodynamics between $La_{0.5}Sr_{0.5}CoO_3$ and CrO_3 is studied for the thermodynamically favorable pathway

employing first principles thermodynamics. The variation of CrO_3 in the reaction is mapped to the partial pressure of CrO_3 and the phase diagram of the reaction is extracted. We find that the CrO_3 concentration significantly alters the reaction products. We observe that the formation of the Cr poisoning by-product, $SrCrO_4$ is favored for a wide range of experimental CrO_3 partial pressures and temperatures agreeing with experimental observations. In addition, our study provides a prediction for experimental P-T conditions to avoid Cr poisoning effects in LSCO. This method can be extended to identify reaction energetics of other multicomponent systems as well.

Acknowledgments

This work is supported, in part, through a grant from the Office of Fossil Energy, U.S. Department of Energy (DE-FE-0009682). The authors acknowledge partial computational support through the Extreme Science and Engineering Discovery Environment (XSEDE).

References

[1] B.C.H. Steele, A. Heinzel, Materials for fuel-cell technologies, Nature 414 (6861) (2001) 345–352.
[2] D. Lee, Y.-L. Lee, W.T. Hong, M.D. Biegalski, D. Morgan, Y. Shao-Horn, Oxygen surface exchange kinetics and stability of $(La,Sr)_2CoO_{4\pm\delta}$, $La_{1x}Sr_xMO_{3-\delta}$(M = Co and Fe), J. Mater. Chem. A 3 (5) (2015) 2144–2157.
[3] E.A. Ahmad, L. Liborio, D. Kramer, G. Mallia, A.R. Kucernak, N.M. Harrison, Thermodynamic stability of $LaMnO_3$ and its competing oxides: a hybrid density functional study of an alkaline fuel cell catalyst, Phys. Rev. B 84 (8) (2011) 085137.
[4] Y.-M. Kim, J. He, M.D. Biegalski, H. Ambaye, V. Lauter, H.M. Christen, S.T. Pantelides, S.J. Pennycook, S.V. Kalinin, A.Y. Borisevich, Probing oxygen vacancy concentration and homogeneity in solid-oxide fuel-cell cathode materials on the subunit-cell level, Nat. Mater. 11 (10) (2012) 888–894.
[5] Y.A. Mastrikov, R. Merkle, E.A. Kotomin, M.M. Kuklja, J. Maier, Formation and migration of oxygen vacancies in $Ba_{1-x}Sr_xCo_{1-y}Fe_yO_{3-\delta}$ perovskites: insight from ab initio calculations and comparison with $Ba_{1-x}Sr_xCo_{1-y}Fe_yO_{3-\delta}$, Phys. Chem. Chem. Phys. 15 (3) (2013) 911–918.
[6] M.M. Kuklja, E.A. Kotomin, R. Merkle, Y.A. Mastrikov, J. Maier, Combined theoretical and experimental analysis of processes determining cathode performance in solid oxide fuel cells, Phys. Chem. Chem. Phys. 15 (15) (2013) 5443–5471.
[7] C.-W. Lee, S.B. Sinnott, E.D. Wachsman, R. Devanathan, First-principles calculations of $(La,Sr_x)(Co_y,Fe)O_3$ (LSCF) solids and surfaces, Summer Res. Inst. Interfacial Condensed Phase Chem. Phys. (2006) 171.
[8] C.-W. Lee, R.K. Behera, E.D. Wachsman, S.R. Phillpot, S.B. Sinnott, Stoichiometry of the $LaFeO_3$ (010) surface determined from first-principles and thermodynamic calculations, Phys. Rev. B 83 (11) (2011) 115418.
[9] C.-W. Lee, R.K. Behera, S. Okamoto, R. Devanathan, E.D. Wachsman, S.R. Phillpot, S.B. Sinnott, Stabilization mechanisms of $LaFeO_3$ (010) surfaces determined with first principles calculations, J. Am. Ceram. Soc. 94 (6) (2011) 1931–1939.
[10] A.J. Jacobson, Materials for solid oxide fuel cells, Chem. Mater. 22 (3) (2010) 660–674.
[11] T. Horita, Y. Xiong, H. Kishimoto, K. Yamaji, M.E. Brito, H. Yokokawa, Chromium poisoning and degradation at $(La,Sr)MnO_3$ and $(La,Sr)FeO_3$ cathodes for solid oxide fuel cells, J. Electrochem. Soc. 157 (5) (2010) B614.
[12] E. Bucher, M. Yang, W. Sitte, In situ investigations of the chromium-induced degradation of the oxygen surface exchange kinetics of IT-SOFC cathode materials $La_{0.6}Sr_{0.4}CoO_{3-\delta}$ and $La_{0.58}Sr_{0.4}Co_{0.2}Fe_{0.8}O_{3-\delta}$, J. Electrochem. Soc. 159 (5) (2012) B592.
[13] W. Guan, L. Jin, W. Wu, Y. Zheng, G. Wang, W.G. Wang, Effect and mechanism of Cr deposition in cathode current collecting layer on cell performance inside stack for planar solid oxide fuel cells, J. Power Sources 245 (2014) 119–128.
[14] E. Park, S. Taniguchi, T. Daio, J.-T. Chou, K. Sasaki, Comparison of chromium poisoning among solid oxide fuel cell cathode materials, Solid State Ionics 262 (2014) 421–427.
[15] M. Kornely, N.H. Menzler, A. Weber, E. Ivers-Tiffée, Degradation of a high performance SOFC cathode by Cr-poisoning at OCV-conditions, Fuel Cells 13 (4) (2013) 506–510.
[16] S.P. Jiang, X. Chen, Chromium deposition and poisoning of cathodes of solid oxide fuel cells – a review, Int. J. Hydrogen Energy 39 (1) (2014) 505–531.
[17] X. Chen, Y. Zhen, J. Li, S.P. Jiang, Chromium deposition and poisoning in dry and humidified air at $(La_{0.8}Sr_{0.2})_{0.9}MnO_{3+\delta}$ cathodes of solid oxide fuel cells, Int. J. Hydrogen Energy 35 (6) (2010) 2477–2485.
[18] S.P. Jiang, J.P. Zhang, L. Apateanu, K. Foger, Deposition of chromium species at Sr-doped $LaMnO_3$ electrodes in solid oxide fuel cells. I. Mechanism and kinetics, J. Electrochem. Soc. 147 (11) (2000) 4013.
[19] S. Badwal, R. Deller, K. Fogera, Y. Ramprakash, Interaction between chromia forming alloy interconnects electrode of solid oxide fuel cells, Solid State Ionics 99 (1997) 297–310.
[20] H.N. Sharma, V. Sharma, A.B. Mhadeshwar, R. Ramprasad, Why Pt survives but Pd suffers from SO_x poisoning?, J Phys. Chem. Lett. 6 (7) (2015) 1140–1148.
[21] A.R. Akbarzadeh, V. Ozoliņš, C. Wolverton, First-principles determination of multicomponent hydride phase diagrams: application to the Li-Mg-N-H system, Adv. Mater. 19 (20) (2007) 3233–3239.
[22] A.R. Akbarzadeh, C. Wolverton, V. Ozolins, First-principles determination of crystal structures, phase stability, and reaction thermodynamics in the Li-Mg-Al-H hydrogen storage system, Phys. Rev. B 79 (18) (2009) 184102.
[23] Y. Duan, B. Zhang, D.C. Sorescu, J.K. Johnson, CO_2 capture properties of M-C-O-H (M=Li, Na, K) systems: a combined density functional theory and lattice phonon dynamics study, J. Solid State Chem. 184 (2) (2011) 304–311.
[24] V. Sharma, M.K. Mahapatra, S. Krishnan, Z. Thatcher, B.D. Huey, P. Singh, R. Ramprasad, Effects of moisture on (La, A)MnO_3 (A = Ca, Sr, Ba) solid oxide fuel cell cathodes: a first-principles and experimental study, J. Mater. Chem. A (2016) 5605–5615.
[25] V. Sharma, M.K. Mahapatra, P. Singh, R. Ramprasad, Cationic surface segregation in doped $LaMnO_3$, J. Mater. Sci. 50 (8) (2015) 3051–3056.
[26] D. Fuks, Y. Mastrikov, E. Kotomin, J. Maier, Ab initio thermodynamic study of (Ba,Sr)(Co,Fe) O_3 perovskite solid solutions for fuel cell applications, J. Mater. Chem. A 1 (2013) 14320–14328.
[27] J. Mastin, M.A. Einarsrud, T. Grande, Structural and thermal properties of $La_{1-x}Sr_xCoO_{3-\delta}$, Chem. Mater. 18 (25) (2006) 6047–6053.
[28] L.W. Tai, M.M. Nasrallah, H.U. Anderson, D.M. Sparlin, S.R. Sehlin, Structure and electrical properties of $La_{1-x}Sr_xCo_{1-y}Fe_yO_3$. Part 2. The system $La_{1-x}Sr_xCo_{0.2}Fe_{0.8}O_3$, Solid State Ionics 76 (3–4) (1995) 273–283.
[29] S. Zhang, N. Han, X. Tan, Density functional theory calculations of atomic, electronic and thermodynamic properties of cubic $LaCoO_3$ and $La_{1-x}SrCoO_3$ surfaces, RSC Adv. 5 (2015) 760–769.
[30] M.W. Penninger, C.H. Kim, L.T. Thompson, W.F. Schneider, DFT analysis of NO oxidation intermediates on undoped and doped $LaCoO_3$ perovskite, J. Phys. Chem. C 119 (35) (2015) 20488–20494.
[31] H. Zhu, C. Tang, R. Ramprasad, Phase equilibria at Si-HfO_2 and Pt-HfO_2 interfaces from first principles thermodynamics, Phys. Rev. B 82 (23) (2010) 235413.
[32] D.R. Stull, H. Prophet, JANAF Thermochemical Tables, Tech. Rep., DTIC Document, 1971.
[33] G. Kresse, J. Furthmüller, Efficiency of ab-initio total energy calculations for metals and semiconductors using a plane-wave basis set, Comput. Mater. Sci. 6 (1) (1996) 15–50.
[34] G. Kresse, J. Furthmüller, Efficient iterative schemes for ab initio total-energy calculations using a plane-wave basis set, Phys. Rev. B 54 (16) (1996) 11169–11186.
[35] J.P. Perdew, K. Burke, M. Ernzerhof, Generalized gradient approximation made simple, Phys. Rev. Lett. 77 (18) (1996) 3865–3868.
[36] P.E. Blöchl, Projector augmented-wave method, Phys. Rev. B 50 (24) (1994) 17953–17979.
[37] L. Wang, T. Maxisch, G. Ceder, Oxidation energies of transition metal oxides within the GGA+U framework, Phys. Rev. B 73 (19) (2006) 195107.
[38] A. Jain, G. Hautier, C.J. Moore, S. Ping Ong, C.C. Fischer, T. Mueller, K.A. Persson, G. Ceder, A high-throughput infrastructure for density functional theory calculations, Comput. Mater. Sci. 50 (8) (2011) 2295–2310.
[39] Y.-L. Lee, J. Kleis, J. Rossmeisl, D. Morgan, Ab initio energetics of $LaBO_3$(001) (B=Mn, Fe, Co, and Ni) for solid oxide fuel cell cathodes, Phys. Rev. B 80 (22) (2009) 224101.
[40] V.I. Anisimov, F. Aryasetiawan, A.I. Lichtenstein, First-principles calculations of the electronic structure and spectra of strongly correlated systems: the LDA + U method, J. Phys. Condens. Matter 9 (4) (1997) 767–808.
[41] C. Franchini, R. Podloucky, J. Paier, M. Marsman, G. Kresse, Ground-state properties of multivalent manganese oxides: density functional and hybrid density functional calculations, Phys. Rev. B 75 (19) (2007) 195128.
[42] L. Ge, A. Verma, R. Goettler, D. Lovett, R.K.S. Raman, P. Singh, Oxide scale morphology and chromium evaporation characteristics of alloys for balance of plant applications in solid oxide fuel cells, Metall. Mater. Trans. A 44 (1) (2013) 193–206.